NOx conversion on LSM15-CGO10 cell stacks with BaO impregnation

Traulsen, Marie Lund; Andersen, Kjeld Bøhm; Kammer Hansen, Kent

Published in:
Journal of Materials Chemistry

Link to article, DOI:
10.1039/c2jm31417g

Publication date:
2012

Journal Name

Dynamic Article Links ►

Cite this: DOI: 10.1039/c0xx00000x

www.rsc.org/xxxxxx

ARTICLE TYPE

NO_x conversion on LSM15-CGO10 cell stacks with BaO impregnation

Marie Lund Traulsen,* Kjeld Bøhm Andersen and Kent Kammer Hansen

Received (in XXX, XXX) Xth XXXXXXXXX 20XX, Accepted Xth XXXXXXXXX 20XX
DOI: 10.1039/b000000x

The electrochemical conversion of NO_x on non-impregnated and BaO-impregnated LSM15-CGO10 ($La_{0.85}Sr_{0.15}MnO_3$-$Ce_{0.9}Gd_{0.1}O_{1.95}$) porous cell stacks has been investigated, and extensive impedance analysis have been performed to identify the effect of the BaO on the electrode processes. The investigation was conducted in the temperature range 300-500 °C, a polarisation range from 3 V to 9 V and in atmospheres containing 1000 ppm NO, 1000 ppm NO + 10% O_2 and 10% O_2. On the non-impregnated cell stacks no NO_x conversion was observed at any of the investigated conditions. However, BaO impregnation greatly enhanced the NO_x conversion and at 400 °C and 9 V polarisation a BaO-impregnated cell stack showed 60% NO_x conversion into N_2 with 8% current efficiency in 1000 ppm NO + 10% O_2. This demonstrates high NO_x conversion can be achieved on an entirely ceramic cell without expensive noble metals. Furthermore the NO_x conversion and current efficiency was shown to be strongly dependent on temperature and polarisation. The impedance analysis revealed that the BaO-impregnation increased the overall activity of the cell stacks, but also changed the adsorption state of NO_x on the electrodes; whether the increased activity or the changed adsorption state is mainly responsible for the improved NO_x conversion remains unknown.

Introduction

In Europe the NO_x-emission from the road transport has been significantly reduced during the last 10 years, mainly due to the introduction of the three-way-catalyst on gasoline vehicles[1]. Due to the negative impact of NO_x-emissions on both human health and the environment[2], a further reduction in the NO_x emissions from the car fleet is desirable. However a major challenge in that connection is the increased number of diesel vehicles, as the conventional three-way-catalyst is incapable of removing NO_x from diesel exhaust. For this reason much research is currently focused on NO_x-removal technologies for diesel exhaust, the most heavily investigated technologies being selective catalytic reduction with ammonia (NH_3-SCR), selective catalytic reduction with hydrocarbons (HC-SCR) and the NO_x-storage and reduction (NSR) catalyst[3]. In all these three technologies there is the need for a reducing agent, either coming from operating the engine occasionally in an excess fuel to air-ratio (HC-SCR and NSR) or supplied by a separate system (NH_3-SCR). A NO_x removal technology without the need for the addition of a reducing agent would be simpler and therefore advantageous compared to the aforementioned technologies.

A suggestion for such a technology is electrochemical NO_x removal, where the NO_x is reduced to N_2 and O_2 by electrons supplied to a polarised electrode[4]. The technology is inspired by the finding in 1975 by Pancharatnam et al.[5] that NO can be reduced to N_2 during polarisation of a zirconia based cell in the absence of oxygen, and later it was shown by Cicero et al.[6] and Hibino et al.[7] that NO_x also could be electrochemically reduced in the presence of oxygen. Since then several studies has been made in the field of electrochemical deNO_x by different research groups[6-13]. For electrochemical NO_x removal to become a technology of practical interest, a first and major obstacle to be overcome is to find electrode materials with a sufficiently high activity and selectivity for NO_x reduction[4].

With respect to selectivity the major problem is the competing reduction of O_2; in eq. 1 the desired NO reduction on the cathode is stated and the competing O_2 reduction is stated in Eq. 2.

$$NO + 2\,e^- \rightarrow \frac{1}{2}N_2 + O^{2-} \qquad \text{Eq. 1}$$

$$\frac{1}{2}O_2 + 2\,e^- \rightarrow O^{2-} \qquad \text{Eq. 2}$$

In this work it is investigated if the conversion of NO_x at 300-500 °C on LSM15-CGO10 composite electrodes can be increased by impregnating the electrodes with BaO. BaO is the most commonly used NO_x storage compound in the NSR catalyst[14], and the idea in this work is to increase the NO_x conversion by up-concentrating the NO_x on the electrode surface in the form of $Ba(NO_3)_2$. Previous work by Li et al.[15] and Yoshinobu et al.[16] have shown good results from combining BaO and electrochemical deNO_x, but in both cases the investigated electrode systems contained Pt or other noble metals, which increases the cost of the system. The work by Simonsen et al.[17] showed LSM15 in combination with Ba could be an efficient catalyst for electrochemical NO_x removal; however the work did not include any conversion measurements. Conversion measurements are included in this work, where electrochemical NO_x removal is investigated on an entirely ceramic system, i.e. a system without expensive noble metals. LSM15 is chosen as electrode material for this investigation, as LSM15 has good stability compared to other perovskites like $La_{1-x}Sr_xFe_{1-y}Co_yO_3$ and $Ba_{1-x}Sr_xFe_{1-y}Co_yO_3$, eventhough these have a higher activity in the investigated temperature range[18]. CGO10 was chosen as electrolyte and component in the electrode, as the ionic conductivity of CGO10 is superior to the ionic conductivity of YSZ (Yttria Stabilized Zirconia) below 600 °C[19]. The non-impregnated and BaO-impregnated electrodes were investigated in a set-up with a porous 11-layer cell stack, as the large contact area between gas flow and cell stack in this set-up increases the conversion and makes it easy to detect any changes in the gas composition. Two complementary approaches were used to investigate the effect of the BaO-impregnation on the electrode performance. The one approach involved measurements of the NO_x conversion as function of temperature, polarisation and gas composition. This approach was supplemented by an extensive impedance analysis aimed at clarifying which processes contributed to the polarisation resistance of the cell stacks, and how these processes were affected by the BaO impregnation.

Experimental:

Cell stack fabrication:

The 11-layer porous cell stacks consisted of 11 alternating layers of composite electrode (65 wt% LSM15 (Haldor Topsøe) and 35 wt% CGO10 (Rhodia)) and electrolyte (CGO10). The porous composite electrode layers were manufactured by mixing LSM15, CGO10, solvent (mixture of ethanol and butanone), binder (polyvinylbuyral), dispersant (polyvinylpyrrolidone) and pore former (graphite) into a slurry, ball mill the slurry and thereafter tape caste the slurry into green tapes of approximately 40 μm thickness, for more details see Hee et al [20]. The porous CGO10 layers were prepared in a similar manner, and subsequent the green electrode and electrolyte layers were laminated together and round cell stacks were stamped out. The cell stacks were sintered with the

maximum temperature 1250 °C held for 4 hours and thereby achieved a diameter of ≈14 mm. Prior to mounting in the test-setup the cell stacks were painted with gold paste (ESL Electro-Science) mixed with 20% carbon (Graphit Kropfmühl AG), which was burned off at 800 °C in order to create porous gold current collectors on each side of the cell stack.

Impregnation

For impregnation of the porous cell stacks with BaO a 0.3 M aqueous $Ba(NO_3)_2$ (Merck) solution with 10 wt% P123 (BASF) was prepared. The cell stacks were covered with the $Ba(NO_3)_2$ solution and put under vacuum for ≈10 s, whereafter excess impregnation solution was wiped of the surface. The impregnated cell stacks were then heated to 700 °C for 1 h to decompose the $Ba(NO_3)_2$ into BaO. 700 °C was chosen to assure total

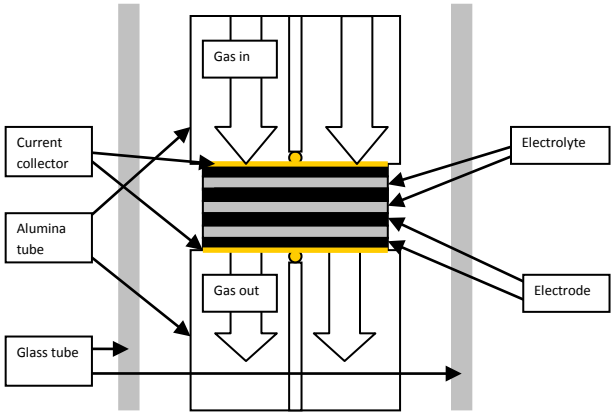

Fig. 1 Sketch of test-setup for porous 11-layer cell stack. Reprinted with permission from Werchmeister et al. 2010[13]

decomposition, since a DTA experiments showed $Ba(NO_3)_2$ decomposed at 600-640 °C, even though the decomposition temperature reported by literature in general were lower, in the range 500-600 °C [21-23].

Test-setup

For electrochemical cell testing the stack was mounted in between two alumina tubes, which contained channels for the gas flow and measurement probes for the electrochemical characterization. The cell and the alumina tubes were inclosed in a quartz tube and mounted vertically in a furnace. A sketch of the set-up is shown in Fig. 1.

Electrochemical Testing and Conversion measurements:

During the tests the cell stacks were characterized by electrochemical impedance spectroscopy (EIS). The impedance spectra were recorded with a Gamry Reference 600 potentiostat in the frequency range 1 MHz to 0.001 Hz with 6 points pr. decade and 36 mV rms amplitude. The Gamry Reference 600 potentiostat was also used for polarisation of the cells during the conversion measurements. During the experiments the outlet gas from the cell stack was constantly monitored. The NO and NO_2 concentrations were monitored by a chemiluminiscense detector Model 42*i* High Level from Thermo Scientific, while the N_2, N_2O and O_2 concentrations were monitored with a mass spectrometer from Pfeiffer Vacuum, type Omnistar GSD 301SEM. In total five cell stacks were tested, two non-impregnated stacks named N1 and N2, and three BaO-impregnated stacks named B1, B2 and B3.

Test conditions

The conversion measurements were made at the flow rate 2 L/h in 1000 ppm NO and 1000 ppm NO + 10% O_2 in both cases with balance Ar. These concentrations of NO and O_2 were chosen as they resemble the concentrations which may be found in the exhaust from a diesel car[24]. It should be noted, that 1000 ppm NO + 10% O_2 are the concentrations set during the experiments, while in reality the gas composition will contains some NO_2 due to the equilibrium NO + ½ O_2 ⇆ NO_2. Moreover impedance measurements were recorded in 10% O_2 with balance Ar for comparison to impedance spectra recorded in NO containing atmospheres. The experiments were carried out in the temperature range 300-500 °C which is close to the expected temperature of diesel engine

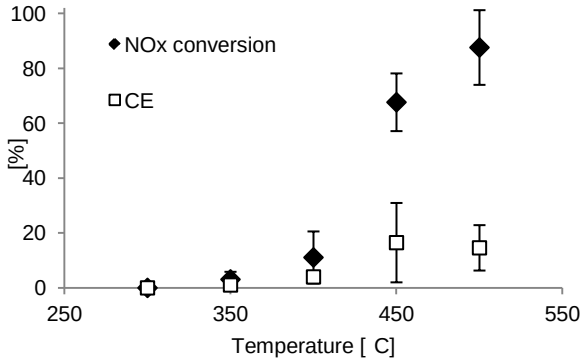

Fig. 2 Percentage of NO_x converted into N_2 and the current efficiency (CE) during 3 V polarisation for 2 h in 1000 ppm NO on a BaO impregnated cell stack.

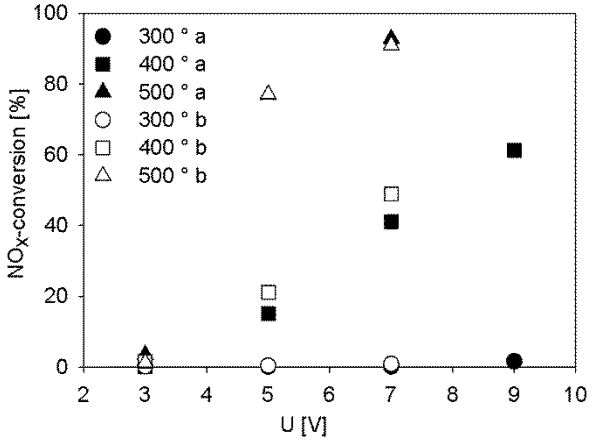

Fig. 3 Percentage of NO_x converted into N_2 during polarisation for 2 h in 1000 ppm NO + 10% O_2 on a BaO impregnated cell stack. Closed symbols labelled a were recorded during the stepwise voltage increase from 3 to 9 V, while open symbols labelled b were recorded during the subsequent voltage decrease from 9 V to 3 V.

exhaust of 100-400 °C[25]. Polarisation experiments were made in the range 3-9 V. As each 11 layer cell stacks contain 5 "cells", the polarisation range pr. cell was 0.6-1.8 V.

SEM

Before and after testing the cell stacks were examined in a Zeiss Supra 35 scanning electron microscope equipped with a field emission gun. In order to obtain high magnification images of the electrode microstructure images were recorded with the in-lens detector and 3 keV acceleration voltage on cells just broken and put directly into the microscope.

Results

Conversion and current efficiency

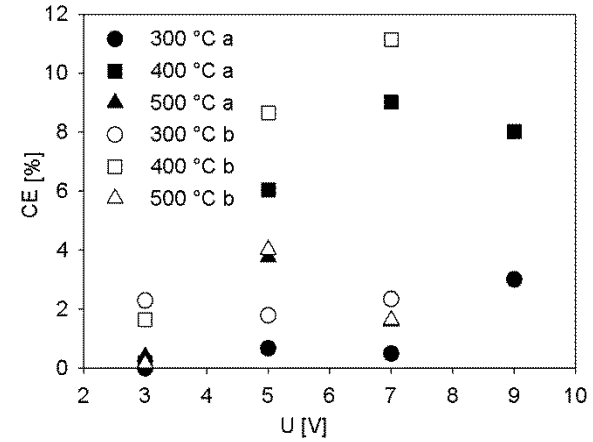

Fig. 4 Current efficiency for conversion of NO_x into N_2 during polarisation for 2 h in 1000 ppm NO + 10% O_2 on a BaO impregnated cell stack. Closed symbols labelled a were recorded during the stepwise voltage increase from 3 to 9 V, while open symbols labelled b were recorded during the subsequent voltage decrease from 9 V to 3 V.

On the non-impregnated cell stacks no conversion of NO into N_2 was observed during 3 V polarisation in the temperature range 300-500 °C, neither when the cell stacks were supplied with 1000 ppm NO + 10% O_2 nor when the stacks were supplied with only 1000 ppm NO. However, on the BaO impregnated cell stacks conversion of NO_x into N_2 was observed both without presence of O_2 and in the presence of 10% O_2. In Fig. 2 the results from the conversion measurement without O_2 in 1000 ppm NO on the BaO impregnated stacks are stated, the results are based on measurements on three different stacks. Fig. 2 shows the NO_x conversion increases with temperature, and especially from 400 °C to 450 °C a significant increase in the conversion is observed from below 20% to above 60%. A significant increase in the current efficiency is also observed from 400 to 450 °C, as the current efficiency increases from 4% to 16%.

When the BaO impregnated cell stacks were supplied with 1000 ppm NO + 10% O_2 and polarised at 3 V the NO_x conversion also increased with temperature, however the average NO_x conversion achieved at 500 °C was only 4% and the corresponding current efficiency only 0.3%.

On one of the BaO impregnated cell stacks the influence of varying the polarisation between 3 V, 5 V, 7 V and 9 V was investigated at 300 °C, 400 °C and 500 °C. At each temperature the first measurements was made at 3 V whereafter the voltage was increased stepwise till 9 V was reached, each time with the voltage kept at the specified value for one hour, with a one hour break at OCV in between. After 9 V had been reached the measurements at 7 V, 5 V and 3 V were repeated while going down in voltage. The results for the NO_x conversion are shown in Fig. 3 and for the current efficiency in Fig. 4. With respect to the NO_x-conversion, only a negligible effect of increasing the voltage is observed at 300 °C, where the NO_x conversion only

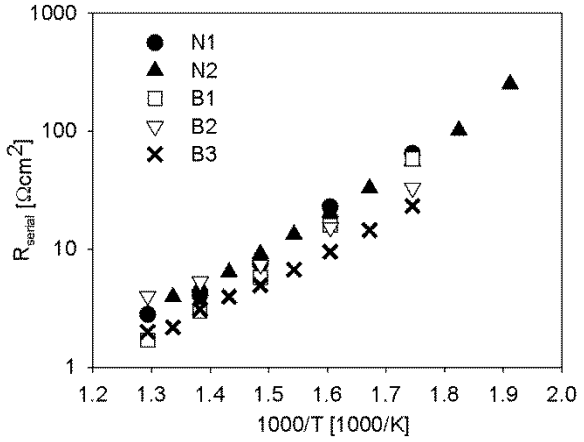

Fig. 5 Arrhenious plot of the serial resistance obtained from fitting of impedance spectra recorded in 1000 ppm NO + 10% O_2 on non-impregnated (N1 and N2) and BaO-impregnated (B1, B2 and B3) cell stacks.

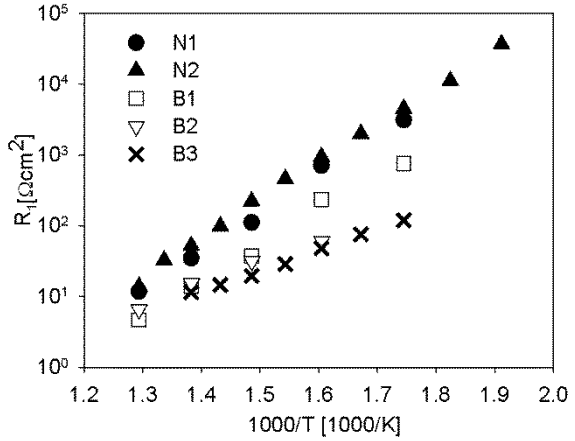

Fig. 6 Arrhenious plot of the high frequency process resistance obtained from fitting of impedance spectra recorded in 1000 ppm NO + 10% O_2 on non-impregnated (N1 and N2) and BaO-impregnated (B1, B2 and B3) cell stacks.

increased from 0% at 3 V to 2% at -9 V. Contrary to this a distinct effect is observed from increasing the voltage at 400 °C, where the NO_x conversion increased from 0% at 3 V to 61% at 9 V. Moreover an activation effect is observed at 400 °C on both NO_x-conversion and current efficiency, as both had increased when the measurements at 7 V, 5 V and 3 V were repeated during the second half of experiment. For comparison a similar polarisation experiment was made at 400 °C on a non-impregnated cell stack, but no formation of N_2 was observed not

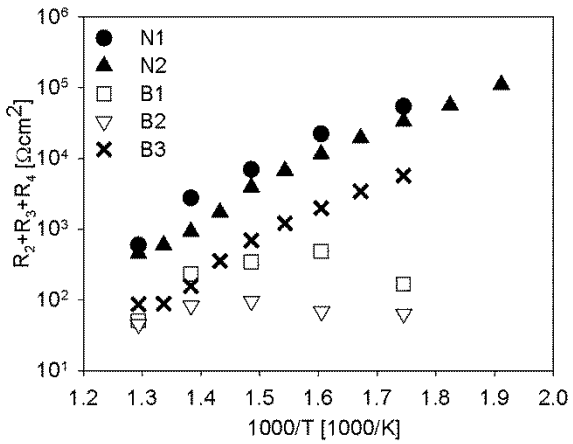

Fig. 7 Arrhenious plot of the sum of the low frequency processes resistance. The resistances were obtained from fitting of impedance spectra recorded in 1000 ppm NO + 10% O_2 on non-impregnated (N1 and N2) and BaO-impregnated (B1, B2 and B3) cell stacks.

even at 9 V polarisation. At 500 °C a distinct effect is again observed from increasing the voltage on the BaO-impregnated stack, the relative largest increase in NO_x conversion per voltage increase is observed when the voltage is increased from 3 V to 5 V, which makes the NO_x conversion increase from 4% to 93%. The measurement at 9 V is missing at 500 °C, as the corresponding current exceeded the maximum current of the Gamry Ref 600 Potentiostat and the experiment for this reason was interrupted. In general with respect to the current efficiencies they appear to be more or less independent on the voltage at 300 °C and 500 °C and do in no cases exceed 5%, whereas at 400 °C the current efficiencies clearly increase with voltage until 7 V, where it reaches a maximum value of ≈10%.

Deconvolution of impedance spectra

The impedance spectra recorded on the non-impregnated and the BaO-impregnated cell stack were all fitted with a serial resistance and a series connection of 3-4 sub circuits, each sub circuit containing a resistance and a constant phase-element in parallel. In general the process located at the highest frequencies was clearly separable from the lower frequency processes, which on the other hand were strongly overlapping in the impedance spectra. Due to the strong overlap in the low frequency region it was not possible to obtain a linear Arrhenious plot for the individual resistances in this frequency region. To enlighten the processes in the low frequency region the sum of the low frequency resistances (R_2, R_3 and in some cases R_4) were instead plottet together. The Arrhenious plot of the serial resistance, R_1 and $R_2+R_3+R_4$ are shown in Fig. 5, Fig. 6 and Fig. 7 respectively.

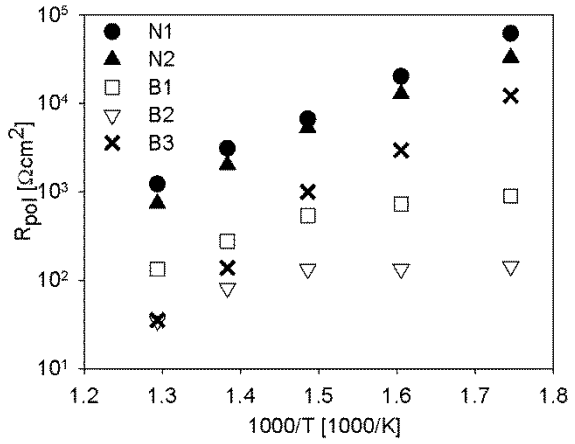

Fig. 8 Polarisation resistance of non-impregnated and impregnated cell stacks in 10% O_2

The serial resistance of the two non-impregnated cell stacks are in almost exact agreement, which is also the case for the resistance of the high frequency process (R_1) and the low frequency processes (R_2+R_3+R_4). This means good reproducibility is obtained for the non-impregnated cell stacks. The serial resistances of the BaO-impregnated cell stacks are very close to those of the non-impregnated, however with a tendency to be slightly lower. For the high frequency process the serial resistance is consequently lower for the impregnated cell stacks, the difference between non-impregnated and impregnated stacks being largest at low temperatures. For the low frequency processes some discrepancy is observed between the impregnated stacks, but in all cases the low frequency resistances are lower on the BaO-impregnated stacks compared to non-impregnated. One of the impregnated stacks (B3) shows an activation energy in the low frequency region similar to the activation energy of the non-impregnated stacks. The two other impregnated stacks show in the low frequency region a quite different behaviour, as the resistance show very little temperature dependency. At the highest measured temperature (500 °C), the resistance of all the impregnated cell stacks are quite equal.

For comparison to the just described resistances in the cell stack in 1000 ppm NO + 10% O_2, the total polarisation resistance in non- and BaO-impregnated cell stacks subjected to only 10% O_2 is shown in Fig. 8. A decrease in the polarisation resistance on the impregnated stacks similar to the one observed in 1000 ppm NO + 10 % O_2 is also observed in 10% O_2. This indicates the BaO impregnation cause a general increase in the activity of the electrodes.

Characteristics of processes

In addition to the impedance spectra recorded during temperature variations impedance spectra were also recorded during variation

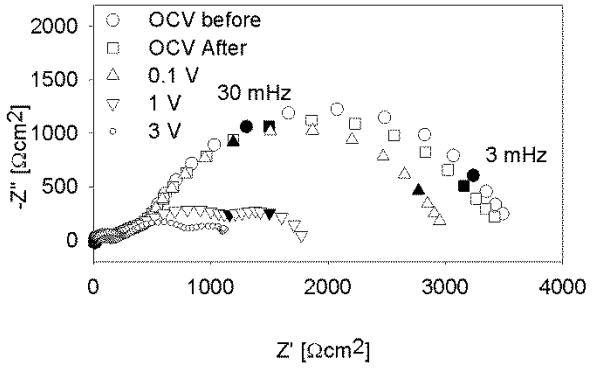

Fig. 9. Impedance spectra recorded on non-impregnated cell stack at OCV and during polarisation. The stack was at 400 °C and supplied with 1000 ppm NO + 10% O_2. The stated frequencies are marked with closed symbols. The spectra labelled "OCV before" and "OCV after" refers are impedance spectra recorded at OCV immediately before and after impedance spectra were recorded under current load.

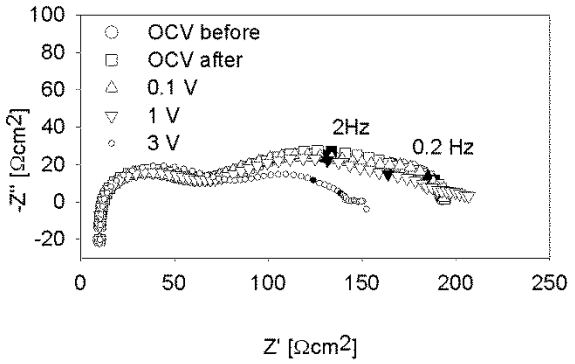

Fig. 10 Impedance spectra recorded on BaO-impregnated cell stack at OCV during polarisation. The stack was at 400 °C and supplied with 1000 ppm NO + 10% O_2. The stated frequencies are marked with closed symbols. The spectra labelled "OCV before" and "OCV after" refers are impedance spectra recorded at OCV immediately before and after impedance spectra were recorded under current load.

in gas composition, flow rate and polarisation. For the concentration variations the "standard" gas composition 1000 ppm NO +10% O_2 was varied first by changing the NO content to 1500 ppm and to 500 ppm while keeping pO_2 constant, whereafter the NO concentration was fixed at 1000 ppm NO

while pO_2 was changed to 5% and 15%. These experiments were repeated at several temperatures on the cell stacks. During flow variations the standard flow 2 L/h was increased to 2.5 L/h and 3 L/h. The majority of the reported impedance spectra were recorded at OCV, but at 400 °C a series of impedance spectra were recorded under 0.1V, 1 V and 3 V polarisation on both the non- and the BaO-impregnated stacks. From the impedance spectra recorded at different conditions different characteristics could be found for the processes contributing to the polarisation resistance. These characteristics are listed for the non-impregnated stacks in Table 1 and for the BaO-impregnated stacks in Table 2. It should be noted the characteristics are stated for the 3 dominating processes observed at all temperatures, while a fourth process occasionally appearing at 500 °C is not included. In addition to the process characteristics listed in the tables the impedance spectra recorded during polarisation on the non-impregnated stack and BaO-impregnated stack are shown in Fig. 9 and Fig. 10 respectively, and show a profound change in the low frequency region during polarisation.

Degradation

On all the cell stacks an impedance spectrum was recorded at 300 °C in 1000 ppm NO + 10% O_2 at the very beginning of the test and at the end of the test, i.e. after the temperature variations, polarisation experiments etc, had been performed. From these spectra the serial and polarisation resistances were determined (Table 3) and the percentage change in R_s, R_1 and $R_2+R_3+R_4$ during the cell tests was calculated (Table 4). The non-impregnated cell stacks and one of the BaO impregnated cell stacks (B3) activated during the cell test, as both R_s, R_1 and $R_2+R_3+R_4$ decreased. A decrease in R_s indicates an improved electric contact through the cell stack, but as the percentage change in the polarisation resistance differs from the percentage change in the serial resistances, improved contact cannot solely explain the changes observed in the polarisation resistances. The two BaO impregnated cell stacks, which had the lowest polarisation resistance in the beginning of the test (B1 and B2), degraded during the test which caused a large increase in the resistance of the low frequency processes, while R_s and R_1 decreased during the tests decreased as for the other cell stacks. It is worth noticing, that even though the BaO impregnated cell stacks have a very different initial performance and degradation behaviour, they all at the end of the cell test have a polarisation resistance significantly below the polarisation resistance of the non-impregnated stacks.

SEM microscopy

Representative SEM images from the microscopy investigation of the electrodes are shown in Fig. 11. The SEM images of the non-impregnated electrodes before test (Fig. 11, a) show slightly rugged LSM15 grains in between smooth CGO10 grains. No evident differences are observed between the non-impregnated electrode before test (Fig. 11, a) and after test (Fig. 11, b). On the BaO impregnated electrodes before test (Fig. 11, c), the impregnated BaO is clearly visible as distinct particles located on the LSM15 grains. After testing the microstructure of the BaO impregnated electrodes had clearly changed, and three different kinds of microstructure were observed even within the same cell stack: electrode grains being almost entirely covered by nanometer sized, round and well-defined particles (Fig. 11, d), electrode grains covered in a more "fluffy" structure (Fig. 11, e) and electrode grains covered entirely in flake-like particles (Fig. 11, f). The weight load of BaO on the cell stacks used for the microscopy was 2±0.1wt%, which means differences in microstructure likely cannot be ascribed to differences in BaO weight load. Furthermore the SEM images showed a similar microstructure of the B1 and the B3 cell stacks, even though these stacks degraded/activated quite differently during the testing.

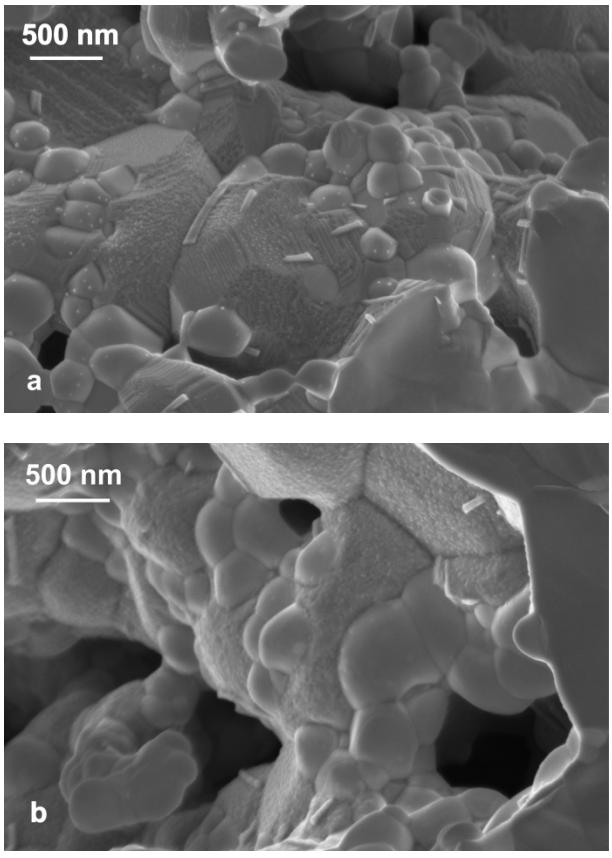

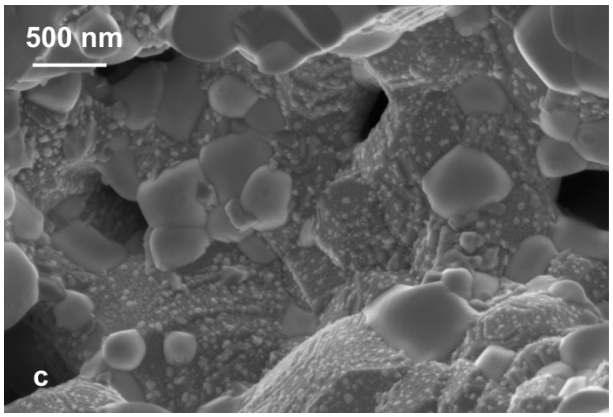

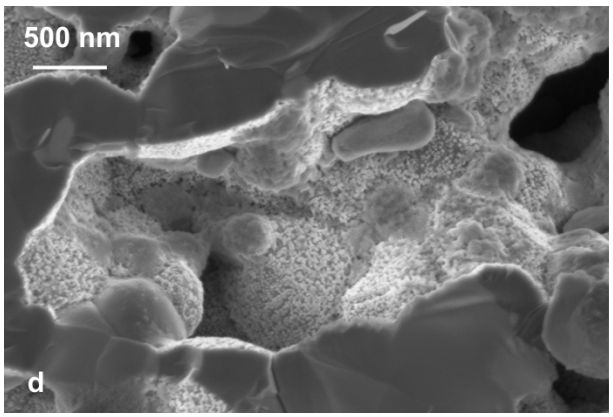

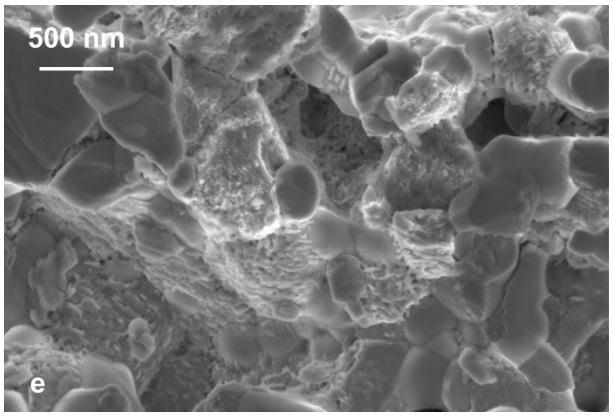

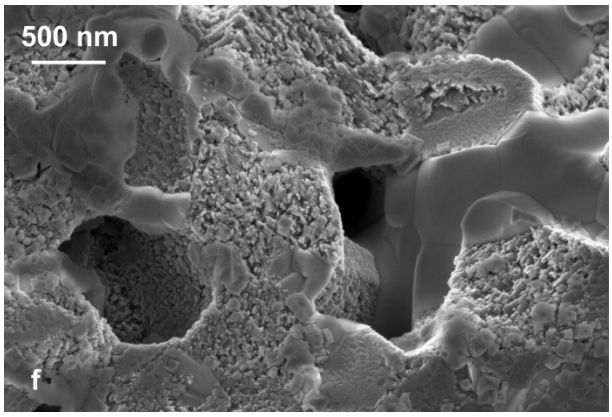

Fig. 11 . SEM images of electrodes of the following LSM15-CGO10 cell stacks: a) non-impregnated before test b) non-impregnated after test c) BaO impregnated before test and d) - f) BaO impregnated after test.

Discussion

Processes on non-impregnated electrodes

Three processes were dominating the polarisation resistance of the non-impregnated electrodes. The high-frequency process was characterized by a temperature independent C_ω with a value around $1 \cdot 10^{-7}$ F/cm^2, a resistance independent on atmosphere and an activation energy of 1.08±0.01eV in 1000 ppm NO + 10% O_2. These characteristics are consistent with characteristics reported in literature for processes related to transfer of oxygen ions between the perovskite and the electrolyte[26-28]. For the middle frequency process R increased with decreasing pO_2 which indicate O_2 or an O-specie is participating in the middle frequency process. The C_ω of the middle frequency arc varied in the range $1 \cdot 10^{-5}$-$1 \cdot 10^{-4}$ F/cm^2, a range in fairly good agreement with the capacitance associated with adsorption and dissociation of oxygen on composite cathodes[29]. The C_ω of the middle frequency arc showed a strange behaviour with respect to the temperature dependency as the C_ω increases from 300 °C to 400 °C and decreases from 400 °C to 500 °C, the observation was made on two different stacks. The best explanation of this observation is the middle frequency process contains contributions from two different processes, which change relative importance with temperature. The low frequency process is characterized by C_ω increasing with temperature and decreasing pO_2, and R decreasing with polarisation. This is consistent with the low frequency process being dependent on the vacancy concentration of the oxide electrode materials and/or the extension/broadening of the triple phase boundary zone. As the resistance of the low frequency process also increases with decreasing NO concentration, the process is ascribed to a NO_x specie (NO or NO_2) which is adsorbing, diffusing on the surface or participating in charge-transfer

related processes at or near the triple phase boundary. The presence of such a process on perovskite/CGO10 electrodes is in good agreement with previous findings in our group[28, 30].

Processes on impregnated electrodes

The impedance spectra recorded on the BaO-impregnated cell stacks are dominated by three processes. The high frequency process shares several characteristics with the high frequency process observed on the non-impregnated cell stack, namely summit frequency range, a C_ω around $1 \cdot 10^{-7}$ F/cm^2 and lack of dependency on gas composition. Therefore the high frequency arc is ascribed to the same process, as it also seems reasonable the process related to transfer of oxygen ions/intermediates between the perovskite and the electrolyte, should be visible for both non-impregnated and impregnated cell stacks. However, Fig. 6 showed the resistance of the high frequency process is consequently lower for the impregnated stacks. The decrease in the resistance could be related to the profound microstructural changes observed in the BaO impregnated electrodes observed in Fig. 11. The characteristics of the middle frequency arc are C_ω increasing with temperature and decreasing with decreasing pO_2, while R decreases with polarisation. The difference in characteristics between the non-impregnated and BaO-impregnated samples makes it less probable the middle frequency process is the same on the two different kinds of cell stacks. Due to the dependency on temperature and polarisation the middle frequency process on the BaO-impregnated stacks is likely due to a triple phase boundary related process, but exactly which process and which species are involved cannot be determined from the available data. Finally the low frequency process on the BaO-impregnated sample show almost identical characteristics with the low frequency process on the non-impregnated cell stack, the one exception being on the BaO-impregnated sample the C_ω also depend on the pNO. Due to the similar characteristics the process is for the BaO-impregnated cell stack also ascribed to triple-phase boundary related adsorption, diffusion and/or charge transfer involving NO or NO_2. However, an important difference between the non- and BaO-impregnated samples is the resistance of the process is much smaller on the BaO-impregnated samples, for instance at 500 °C approximately an order of magnitude smaller compared to the non-impregnated sample. The difference in the low frequency arc resistance to a large extent explains the decreased resistance in the low frequency region of the impregnated samples observed in Fig. 7. It is suggested the decreased resistance of the low frequency process is due to NO/NO_2 getting adsorbed on the BaO in the form of $Ba(NO_3)_2$ rather than getting adsorbed on the LSM15 and/or CGO10 as in the non-impregnated cell stack. The implication of the difference in adsorption for the entire electrode process and NO_x-reduction will be discussed in the next section.

Effect of BaO-impregnation on electrode processes and NO_x conversion

In the previous two sections the electrode processes on the non-impregnated and the BaO-impregnated cell stacks were identified and compared and it was suggested the difference in electrode processes in 1000 ppm NO +10% O_2 could be explained by NO_x adsorbing either directly on the LSM15-CGO10 or on the BaO. From FTIR studies of NO_x adsorption it is known that NO_x at higher temperatures is adsorbed in the form of NO_3^-, and that the NO_3^- formation is preceded by either NO/O_2 co-adsorption or NO_2 formation and subsequent adsorption, these observations has been made both on CGO10/ceria[31] and perovskites[32]. Moreover it was shown in the work by Werchmeister et al. that NO_2 is an important reaction intermediate in electrochemical deNO_x[28, 33], considering the findings from FTIR studies this is likely because NO_2 must be formed before adsorption/formation of nitrate on the electrode surface can occur, a step which necessarily must preceed the electrochemical reduction. Formation of NO_3^- from NO_2 requires an O^- specie according to the reaction scheme $NO_2 + O^- \rightarrow NO_3^-$ (or presence of an adsorbed O-atom and an electron). For the non-impregnated electrode two of the identified processes were one related to O_2 adsorption and dissociation (Process 2) and one related to NO_x adsorption/diffuse/charge transfer at the triple phase boundary (Process 3). This is in very good agreement with the expected mechanism, were $O^-/O(ads)$ needs to be formed (corresponding to Process 2), before NO_3^- can be formed and react in the triple phase boundary region (corresponding to Process 3). With respect to adsorption of NO_x on BaO and formation of $Ba(NO_3)_2$, this process has been shown by FTIR to proceed fastest with NO_2[34] even though the exact mechanism of $Ba(NO_3)_2$ formation is still under discussion[35-37]. The reaction scheme for $Ba(NO_3)_2$ formation with NO_2 is $BaO + 2\ NO_2 + \frac{1}{2}\ O_2 \rightarrow Ba(NO_3)_2$ and in NSR catalysis this storage process takes place without involving any electrochemical steps. It is suggested that during electrochemical deNO_x the NO_x storage process also takes place without involving any electrochemical steps. This is supported by the fact that the polarisation resistance on the impregnated cell stack show no dependency on O_2 adsorption and dissociation related processes. By combining the results from the impedance analysis with the observation from the conversion measurements, which showed increased NO_x conversion on BaO impregnated cell stacks, it becomes likely that the increased NO_x conversion at least to some extent is due to the adsorption on BaO rather than on LSM15-CGO10, which establishes an easier reaction path for the electrochemical reduction of NO_x in the cell stacks. The suggestion, that the NO_x adsorption on the BaO impregnated cell stack proceeds via a route only dependent on O_2(g) and not electrochemically

enhanced O_2 adsorption/dissociation, does however not explain the increased NO_x conversion in 1000 ppm NO without oxygen. A detailed impedance analysis was not carried out in 1000 ppm NO, as the very low oxygen partial pressure in 1000 ppm NO alters the stochiometry of the oxide electrode materials during time and this instability hinders a reasonable interpretation of the impedance spectra. However, the increased NO_x conversion in 1000 ppm NO could be explained by the general increase in electrode activity caused by the BaO-impregnation. In the results section it was also shown the BaO-impregnation in general caused an increased electrode activity, as the BaO-impregnation also decreased the polarisation resistance in 10% O_2, which is in agreement with the reportings on BaO-containing cathodes being superior in activity to conventional LSM15 cathodes. Therefore it can from this work be concluded, that impregnation with BaO definitely increases the NO_x-conversion on LSM15-CGO10 cathodes, but whether the increased conversion in 1000 ppm NO +10% O_2 mainly is caused by a change in adsorption state or by a general increase in electrode activity remains an unanswered question.

Degradation/activation behaviour of cell stacks related to microstructural changes

The SEM images showed profound changes in the microstructure of the BaO-impregnated cell stacks after testing. The microstructure appeared similar between cell stacks even though they degraded/activated differently during testing. Moreover the images clearly showed areas with different microstructure, which were characterized by 1) Round and well-defined particles, 2) "Fluffy" structure and 3) Flake-like particles. Eventually the differences in microstructure could be different stages of the same process going on the electrodes. A possible explanation of the microstructural changes could be the BaO may react with the electrode materials, LSM15 and/or CGO10, and form new compounds. A possible compound could be $BaCeO_3$ or $BaCe_{1-x}Gd_xO_y$, however it is hard from literature to estimate the risk for $BaCeO_3$ formation. In many studies CGO is used as electrolyte in connection with Ba-containing cathodes and none of the studies report $BaCeO_3$ formation below 900 °C [38-40], however the aforementioned studies only consider the temperature effect on material stability and do not consider the effect of polarisation. With respect to the LSM studies some studies indicate there will be no reaction between Ba-containing compounds and LSM [41, 42] while the work by Yang et al. show Ba diffusing from $Ba_{0.5}Sr_{0.5}Co_{0.8}Fe_{0.2}O_{3-\delta}$ into LSM [43]. In conclusion further microstructural and elemental analysis must be conducted to investigate, if cations have migrated and/or new phases have formed in the BaO-impregnated samples in this work.

Conclusion

The electrochemical conversion of NO_x on non-impregnated and BaO-impregnated LSM15-CGO10 porous cell stacks has been investigated, and extensive impedance analysis have been performed to identify the effect of the BaO on the electrode processes. Non-impregnated LSM15-CGO10 cell stacks were not capable of converting NO_x into N_2 at any of the investigated conditions (300-500 °C, 3 V-9 V polarisation, 1000 ppm NO or 1000 ppm NO + 10% O_2). In contrast BaO impregnated cell stacks could convert NO_x to N_2, even in the presence of 10% O_2, which shows NO_x conversion can be achieved in an entirely ceramic, noble metal-free electrochemical cell. The NO_x conversion to N_2 on the impregnated stacks was significantly enhanced when the temperature was increased from 300 °C to 400 °C or higher, and when the polarisation was increased from 3 V to 5 V or higher. The impedance analysis revealed that the BaO-impregnation both increased the overall activity of the cell stacks and also changed the adsorption state of NO_x on the electrodes, which of the effects are mainly responsible for the increased NO_x conversion remains unknown. The BaO-impregnated cell stacks showed a profound change in microstructure after testing, the cause of this change needs to be investigated further.

Acknowledgement

This work was supported by the Danish Strategic Research Council under contract no. 09-065183. Colleagues at the Fuel Cell and Solid State Chemistry Division, Technical University of Denmark, are thanked for help and fruitful discussions.

Notes and references

Department of Energy Conversion and Storage, Technical University of Denmark, Frederiksborgvej 399, DK-4000 Roskilde, Denmark.
Fax:+45 4677 5858; Tel: +45 2132 7937; E-mail: matr@dtu.dk

References

1 European Environment Agency, *Www. Eea. Europa. Eu*, (accessed 22/12, 2011), .

2 K. Wark, C. F. Warner and W. T. Davis, *Air Pollution its Origin and Control, Third Edition*, Addison Wesley Longman, Inc., USA, 1998.

3 K. Skalska, J. S. Miller and S. Ledakowicz, *Sci. Total Environ.*, 2010, **408,** 3976-3989.

4 K. K. Hansen, *Appl. Catal. , B,* 2010, **100,** 427-432.

5 S. Pancharatnam, R. A. Huggins and D. M. Mason, *J. Electrochem. Soc.*, 1975, **122,** 869-875.

6 D. C. Cicero and L. A. Jarr, *Sep. Sci. Technol.*, 1990, **25,** 1455-1472.

7 T. Hibino, *Chem. Lett.*, 1994, **5,** 927-930.

8 T. Hibino, T. Inoue and M. Sano, *Solid State Ionics*, 2000, **130,** 19-29.

9 K. Hamamoto, Y. Fujishiro and M. Awano, *J. Electrochem. Soc.*, 2008, **155,** E109-E111.

10 K. Hamamoto, T. Suzuki, Y. Fujishiro and M. Awano, *J. Electrochem. Soc.*, 2011, **158,** B1050-B1053.

11 S. Bredikhin, K. Maeda and M. Awano, *Solid State Ionics*, 2001, **144,** 1-9.

12 K. J. Walsh and P. S. Fedkiw, *Solid State Ionics*, 1996, **93,** 17-31.

13 R. M. L. Werchmeister, K. K. Hansen and M. Mogensen, *Mater. Res. Bull.*, 2010, **45,** 1554-1561.

14 W. S. Epling, L. E. Campbell, A. Yezerets, N. W. Currier and J. E. Parks, *Catal. Rev. Sci. Eng.*, 2004, **46,** 163-245.

15 X. Li and P. Vernoux, *Appl. Catal. , B,* 2005, **61,** 267-273.

16 Y. Yoshinobu , Y. Tsuda , H. Ueda , Y. Nakanishi and J. Gong , *SAE Int.J.Fuels Lubr.*, 2010, **3,** 50-60.

17 V. L. E. Simonsen, M. M. Johnsen and K. K. Hansen, *Top. Catal.*, 2007, **45,** 131-135.

18 C. W. Sun, R. Hui and J. Roller, *J. Solid State Electrochem.*, 2010, **14,** 1125-1144.

19 B. Dalslet, P. Blennow, P. V. Hendriksen, N. Bonanos, D. Lybye and M. Mogensen, *J. of Solid State Electrochem.*, 2006, **10,** 547-561.

20 Z. He, K. Bohm, A. L. Keel, F. B. Nygaard, M. Menon and K. K. Hansen, *Ionics*, 2009, **15,** 427-431.

21 S. Gordon and C. Campbell, *Anal. Chem.*, 1955, **27,** 1102-1109.

22 F. Lazarini and B. S. Brcic, *Monatshefte Fur Chemie Und Verwandte Teile Anderer Wissenschaften*, 1966, **97,** 1318-&.

23 A. L. Kustov and M. Makkee, *Appl. Catal. , B,* 2009, **88,** 263-271.

24 J. Kaspar, P. Fornasiero and N. Hickey, *Catal. Today*, 2003, **77,** 419-449.

25 K. Adams, J. Cavataio and R. Hammerle, *Appl. Catal. , B,* 1996, **10,** 157-181.

26 E. Murray, T. Tsai and S. Barnett, *Solid State Ionics*, 1998, **110,** 235-243.

27 M. J. Jørgensen and M. Mogensen, *J. Electrochem. Soc.*, 2001, **148,** A433-A442.

28 R. M. L. Werchmeister, K. K. Hansen and M. Mogensen, *J. Electrochem. Soc.*, 2010, **157,** P35-P42.

29 E. Barsoukov and J. R. Macdonald, *Impedance Spectroscopy Theory, Experiment and Applications, Second Edition*, John Wiley and Sons, Inc., Hoboken, New Jersey, 2005.

30 M. L. Traulsen and K. K. Hansen, *Accepted for Publication in J. of Solid State Electrochem. DOI 10. 1007/s10008-012-1684-9*, 2011, .

31 S. Philipp, A. Drochner, J. Kunert, H. Vogel, J. Theis and E. Lox, *Top. Catal.*, 2004, **30-31,** 235-238.

32 J. Liu, Z. Zhao, C. Xu, A. Duan and G. Jiang, *J. Phys. Chem. C*, 2008, **112,** 5930-5941.

33 R. M. L. Werchmeister, K. K. Hansen and M. Mogensen, *J. Electrochem. Soc.*, 2010, **157,** P107-P112.

34 M. O. Symalla, A. Drochner, H. Vogel, S. Philipp, U. Gobel and W. Muller, *Top. Catal.*, 2007, **42-43,** 199-202.

35 B. Westerberg and E. Fridell, *J. Mol. Catal A: Chem.*, 2001, **165,** 249-263.

36 F. Prinetto, G. Ghiotti, I. Nova, L. Lietti, E. Tronconi and P. Forzatti, *J. Phys. Chem. B*, 2001, **105,** 12732-12745.

37 Y. Ji, T. J. Toops, J. A. Pihl and M. Crocker, *Appl. Catal. , B*, 2009, **91,** 329-338.

38 H. Zhao, D. Teng, X. Zhang, C. Zhang and X. Li, *J. Power Sources*, 2009, **186,** 305-310.

39 J. H. Kim, M. Cassidy, J. T. S. Irvine and J. Bae, *J. Electrochem. Soc.*, 2009, **156,** B682-B689.

40 A. Rolle, N. Preux, G. Ehora, O. Mentre and S. Daviero-Minaud, *Solid State Ionics*, 2011, **184,** 31-34.

41 N. Ai, S. P. Jiang, Z. Lue, K. Chen and W. Su, *J. Electrochem. Soc.*, 2010, **157,** B1033-B1039.

42 C. Jin, J. Liu and J. Sui, *J. Electroceram.*, 2011, **26,** 74-77.

43 M. Yang, M. Zhang, A. Yan, M. Yue, Z. Hou, Y. Dong and M. Cheng, *J. Power Sources*, 2008, **185,** 784-789.

Tables

Table 1. Characteristics of processes contributing to the impedance spectra recorded on non-impregnated cell stacks in an atmosphere containing 500-1500 ppm NO and 5-15% O_2 within the temperature range 300-500 °C.

Process	Freq. range	Characteristic*
1	300-80000 Hz	- C_ω temperature independent
2	0.5-25 Hz	- C_ω increases from 300 to 400 °C, then decreases to 500 °C
		-C_ω dependent on pO_2 (increase with decreasing pO_2)
		- R dependent on pO_2 (increase with decreasing pO_2)
3	0.02-0.5 Hz	- C_ω increases with temperature
		- C_ω dependent on pO_2 (increase with decreasing pO_2)
		- R decreases with polarisation
		- R dependent on pNO (increase with decreasing pNO)

* C_ω is the near-equivalent capacitance of the process

Table 2. Characteristics of processes contributing to the impedance spectra recorded on Ba-impregnated cell stacks in an atmosphere containing 500-1500 ppm NO and 5-15% O_2 within the temperature range 300-500 °C.

Process	Freq. range	Characteristic
1	5000-70000Hz	- C_ω decreases with temperature (9) or increases with temp. (6) and (7)
		- R increases with polarisation
2	8-40 Hz	- C_ω increases with temperature
		- C_ω dependent on pO_2 (decrease with decreasing pO_2)
		- R decreases with polarisation
3	4mHz-0.2 Hz	- C_ω increases with temperature
		- C_ω dependent on pO_2 (increase with decreasing pO_2)
		- C_ω dependent on pNO (increase with decreasing pNO)
		- R decreases with polarisation
		- R dependent on pNO (increase with decreasing pNO)

Table 3. Serial resistance (R_s) and polarisation resistance (R_p) in 1000 ppm NO + 10% O_2 at 300 °C at the start of the test and the end of the test. The values stated for non-impregnated samples are average values for two different tests, the deviation between resistances in the two tests were below 6%.

	Test start		Test end	
	R_s [Ωcm^2]	R_p [Ωcm^2]	R_s [Ωcm^2]	R_p [Ωcm^2]
Non-impregnated	67	46070	48	25320
B1	60	923	30	1090
B2	48	110	38	300
B3	68	66253	44	7643

Table 4. Percentage change in serial resistance (R_s), resistance of the high frequency process (R_1) and the sum of the low frequency processes (R_2+R_3+R_4) between the start and the end of the test. The resistances are obtained from impedance spectra recorded in 1000 ppm NO + 10% O_2 at 300 °C.

	R_s	R_1	R_2+R_3+R_4
Non-impregnated	-29	-91	-39
B1	-50	-83	477
B2	-20	-30	5277
B3	-36	-96	-88